

Drought offsets the positive effect of summer heat waves on the canopy greenness of mountain grasslands

M.C. Corona-Lozada, Samuel Morin, Philippe Choler

▶ **To cite this version:**

M.C. Corona-Lozada, Samuel Morin, Philippe Choler. Drought offsets the positive effect of summer heat waves on the canopy greenness of mountain grasslands. Agricultural and Forest Meteorology, 2019, 276-277, pp.107617. 10.1016/j.agrformet.2019.107617 . hal-02404398

HAL Id: hal-02404398
https://hal.science/hal-02404398

Submitted on 25 Oct 2021

HAL is a multi-disciplinary open access archive for the deposit and dissemination of scientific research documents, whether they are published or not. The documents may come from teaching and research institutions in France or abroad, or from public or private research centers.

L'archive ouverte pluridisciplinaire **HAL**, est destinée au dépôt et à la diffusion de documents scientifiques de niveau recherche, publiés ou non, émanant des établissements d'enseignement et de recherche français ou étrangers, des laboratoires publics ou privés.



Distributed under a Creative Commons Attribution - NonCommercial 4.0 International License

Version of Record: https://www.sciencedirect.com/science/article/pii/S0168192319302254
Manuscript_7f8d73a2f87f993289d325bd1d76af10

Drought offsets the positive effect of summer heat waves on the canopy greenness of mountain grasslands

M.C. Corona-Lozada[1], S. Morin[2] & P. Choler [1,3]

[1] Univ. Grenoble Alpes, Univ. Savoie Mont Blanc, CNRS, LECA, F-38000 Grenoble, France

[2] Univ. Grenoble Alpes, Université de Toulouse, Météo-France, CNRS, CNRM, Centre d'Études de la Neige, F-38000 Grenoble, France

[3] Univ. Grenoble Alpes, Univ. Savoie Mont Blanc, CNRS, LTSER Zone Atelier Alpes, F-38000 Grenoble, France

Corresponding author: Philippe CHOLER

philippe.choler@univ-grenoble-alpes.fr

Tel: +33 4 76 51 48 96

ORCID : 0000-0002-9062-2721

Keywords

Climatic water balance; European Alps; heat wave; MODIS; mountain grasslands; phenology.

© 2019 published by Elsevier. This manuscript is made available under the CC BY NC user license
https://creativecommons.org/licenses/by-nc/4.0/

Abstract (195 words)

Heat waves are becoming more frequent in a warming climate and understanding the impacts of these extreme events on terrestrial ecosystems remains a major challenge. Seasonally snow-covered mountain grasslands are temperature-limited ecosystems and one may question whether the summer heat waves there have the same negative effect on primary productivity as they have on lowland ecosystems. Here, we examined the remotely-sensed phenology of mountain grasslands in the French Alps with a particular focus on the four unusually warm summers that occurred in 2003, 2012, 2015, and 2016. Our results showed that an early and rapid senescence and a lack of late-season regrowth were the most significant responses in 2003 and 2012 when heat waves coincided with climatic water deficit, i.e. negative anomalies of precipitation minus reference evapotranspiration. Mountain grasslands located below 2350m were the most affected. In contrast, we found low senescence and moderate to high regrowth in 2015 and 2016 which were years unaffected by severe water deficit. When water was non-limiting, warm and even very warm summers have a positive effect on the canopy greenness of the highest grasslands, particularly by extending the green period in late summer and early fall. Our study highlights the pivotal role that summer water balance has in the phenological response of mountain grasslands exposed to heat waves.

Introduction

There has been a marked increase in air temperature in the European Alps from the 1980s onwards and this has caused warmer and longer snow-free periods for mountain vegetation (Durand et al., 2009a; Gobiet et al., 2014; Beniston et al., 2018). A growing body of evidence indicates that above treeline ecosystems have undergone significant changes over the last decades, including changes in community composition (Gottfried et al., 2012; Cannone and Pignatti, 2014) and ecosystem functioning (Choler, 2015). Many of these documented changes, such as the upward shift of species (Lenoir et al., 2008; Steinbauer et al., 2018), the thermophilization of high summit flora (Gottfried et al., 2012), or the long-term greening of vegetation at high elevation (Carlson et al., 2017), are consistent with the expected positive effects of rising temperatures in temperature-limited ecosystems. Nonetheless, recent reports indicate that earlier frost exposure due to the earlier snow melt-out date (Wheeler et al., 2014; Liu et al., 2018), more frequent heat waves (Cremonese et al., 2017) and droughts (Marchin et al., 2018) may be additional effects of on-going climate change which could attenuate this positive response. These studies highlighted the need to consider both trends and extreme events when assessing mountain vegetation response to climate change.

In a warming climate, the duration, intensity, and frequency of heat waves is expected to markedly increase (Stocker et al., 2013). The few reports that examine the response of mountain grasslands to summer heat waves have yielded contrasting results. Using both remote sensing and *in situ* measurements, Jolly et al. (2005) found a positive effect of the 2003 heat wave on the summer greenness of high-elevation ecosystems in the Swiss Alps, and this was in stark contrast with what was happening in lowland ecosystems. Cremonese et al. (2017) used flux data and time-lapse cameras to characterize the effect of the 2015 heat wave on a subalpine *Nardus*-rich community and noted a reduction of canopy development in addition to advanced senescence. Experimental approaches using monolith transplantation have highlighted that the negative effect of an increased air temperature only occurred when it coincided with reduced water supply (De Boeck et al., 2016).

This calls for a comparative study that includes a broader range of temperature-precipitation combinations to better capture the interplay of heat waves and drought on mountain grassland phenology.

The remote sensing of vegetation phenology provides a unique opportunity to track ecosystem responses to climate change at a regional scale and over decades (Pettorelli et al., 2005; Richardson et al., 2013). In mountainous environments, several studies have successfully used high or medium resolution satellite images to examine the relationships between climate and the growth response of mountain grasslands (Fontana et al., 2008; Dunn and de Beurs, 2011; Zhang et al., 2013b; Choler, 2015). For seasonally snow-covered ecosystems, the use of snow and vegetation indices may provide several phenological metrics including the onset of growth, the date and magnitude of maximum canopy greenness, the dynamics of senescence, and the date of the first snowfalls. However, many comparative studies (either inter-annual or inter-spatial comparisons) have focused on the maximum or averaged summer greenness and, by doing so, have largely overlooked the late and end of season phenology (Gallinat et al., 2015; Garonna et al., 2018). Yet extreme events occurring after the date of peak standing biomass, such as heat wave or drought, may accelerate the senescence or diminish the possibility of regrowth and this has important consequences for the management of mountain pastures (Nettier et al., 2017). We believe that remotely-sensed phenological metrics that capture the kinetics of both growth and senescence phases will provide a more comprehensive assessment of mountain grassland responses to heat waves.

In this paper, we used time series of the Normalized Difference Vegetation Index (NDVI) for the period 2000 - 2016 to examine how the phenology of mountain grasslands has been impacted by the summer heat waves in 2003, 2012, 2015 and 2016. We performed our comparative analysis by using the NDVI from Moderate-Resolution Imaging Spectroradiometer (MODIS) and meteorological variables derived from the SAFRAN (Système d'Analyse Fournissant des Renseignements Atmosphériques à la Neige) reanalysis system (Durand et al., 2009a, 2009b). We

focused on the French Alps for which the availability of high-resolution land cover data allowed us to select MODIS pixels with predominant coverage of mountain grasslands. More specifically, we addressed the following three sets of questions: (1) what was the intensity, duration, and timing of summer heat waves in the French Alps from 2000 to 2016 and to what extent did these events coincide with climatic water deficit, (2) what are the remotely-sensed indicators that best capture the impact of extreme meteorological events on the phenology of mountain grasslands, and (3) how do heat wave and water balance interfere on the growth and senescence of mountain grasslands?

Materials and Methods

The distribution of mountain grasslands in the French Alps was derived from a 10 m resolution land cover map of France produced by the Centre d'Expertise Scientifique Occupation des sols, downloadable at http://osr-cesbio.ups-tlse.fr/~oso/ (Inglada et al., 2017). To obtain a binary map of mountain grasslands, we aggregated the three land cover classes corresponding to meadows ("pelouses", code 34), heathlands ("landes ligneuses", code 36) and grasslands ("prairies", code 211). We noticed that the class "landes ligneuses" included a limited number of pixels and was not very reliable due to the difficulty in distinguishing mountain low shrubs from nearby grasslands and meadows. We calculated the percent cover of the aggregated class at a 250 m resolution to align with the MODIS data, selecting those pixels with >90% cover and a mean elevation ranging from 1350 m to 2550 m m a.s.l.. This yielded a total of 44,295 pixels which fall into four elevation bands (1350 m - 1650 m, 1650 m - 1950 m, 1950 m - 2250 m, and 2250 m - 2550 m) and 23 SAFRAN massifs (Fig. 1 and Table S1). Pixel-based estimates were averaged by elevation band and massif. This resulted in a table containing 87 combinations of elevation band and massif and 17 years (2000 - 2016). Annual standardized anomalies were calculated from this table.

For meteorological data, we used the SAFRAN reanalysis that simulates surface conditions as a function of elevation in 300 m increments and for 23 massifs of French Alps. These massifs were

defined for their climatological homogeneity in a previous spatial analysis of all weather data available for the French Alps (Durand et al., 2009a; 2009b). The SAFRAN reanalysis was evaluated against in-situ observations by Durand et al. (2009a) and is used for many real-time and climatological applications in the French mountain areas (e.g. Verfaillie et al., 2018). The period from 1981 to 2010 was set as a reference period to estimate standardized anomalies. For each MODIS pixel, we extracted all the required meteorological data to compute a Heat Wave Magnitude index, hereafter HWI, and a Reference Crop Evapotranspiration, hereafter ET_0 as described below..

We simplified the methodology proposed by Russo et al. (2014) to calculate a HWI that accounts for both magnitude and duration of heat waves. First, we identified days exhibiting a maximum temperature above a threshold value. For each day of year (DOY) i, we assembled a dataset (DS_i) comprising the daily Tmax values of the n days before and after day i for the 30 year-long reference period (1981-2010) according to Eq. 1

$$DS_i = \bigcup_{y=1981}^{2010} \bigcup_{i-n}^{i+n} Tmax_{y,i} \qquad (1)$$

where the symbol U denotes the union of values. The 80th percentile of DS_i defined the threshold value for day i. As in Russo et al. (2014), we chose n = 15 days to estimate the threshold. We examined the sensitivity of HWI to varying values of n. The relative change in HWI was predominantly less than 5% when comparing n=15 with n=13, and less than 10% when comparing n=15 with n=11 (Fig. S1). In all cases, the ranking of years was the same and the main findings of the study did not change. Second, we selected all episodes of at least three consecutive days during for which the maximum air temperature exceeded the threshold and summed the daily maximum temperature of each episode to obtain an unscaled magnitude of the heat wave. Finally, we summed the unscaled magnitudes of all heat waves occurring during the three periods of interest (see below).. Compared to Russo et al. (2014), we did not consider sub-heat waves and did not rescale heat wave magnitude into probability values.

ET_0 is a Penman–Monteith estimate of potential evapotranspiration of a reference crop surface that quantifies the evaporating demand of the atmosphere when water is not limiting. We followed the recommendations of the Food and Agricultural Organization (Allen et al., 1998) to compute ET_0 (in mm day^{-1}) from weather data (Eq. 2).

$$ET_0 = \frac{0.408\,\Delta\,(R_n - G) + \gamma \frac{900}{(Tm + 273)}\,u_2(e_s - e_a)}{\Delta + \gamma(1 + 0.34u_2)} \qquad (2)$$

where R_n is the net radiation at crop surface (MJ m^{-2} day^{-1}), G is the soil heat flux density (MJ m^{-2} day^{-1}), Tm is mean daily air temperature at 2 m (°C), u_2 is the wind speed at 2 m (m s^{-1}), e_s is saturation vapour pressure (kPa), e_a is the actual vapour pressure (kPa), Δ is the slope of vapour pressure curve (kPa $°C^{-1}$), and γ is the psychrometric constant (kPa $°C^{-1}$). The use of SAFRAN reanalysis to compute ET_0 according to Eq. 2 is described in Vannier and Braud (2012). The cliamtic water balance corresponding to the difference between precipitation (P) and reference crop evapotranspiration, hereafter P-ET_0, was taken as a proxy to assess the dry–wet conditions of a given period.

For each year, HWI and P - ET_0 were computed over three periods of interest: (i) the climatological summer (June, July and August), hereafter JJA, (ii) the growth phase defined as the 30 days preceding the date of maximum observed NDVI, hereafter B30, and (iii) the senescent phase defined as the 60 days following the date of maximum observed NDVI, hereafter A60 (Fig. 2). We examined the sensitivity of the results to the length of the latter two periods and did not find any significant effect if periods were increased or decreased by 10 to 15 days.

Our remote sensing analysis was based on the surface reflectance acquired by MODIS, a sensor onboard Terra satellite. We downloaded the collection 6 of the MOD09Q1 products, corresponding to tile h18.v4 (40–50◦ N, 0–15.6◦ E), from the Land Processes Distributed Active Archive Center (https://e4ftl01.cr.usgs.gov/). The 8-day composite at 250 m resolution, covering the period from 18 February 2000 to 27 December 2016, was processed following Choler (2015). To

summarize, re-projected surface reflectance values (ρ) in the red and near-infrared (NIR) bandwidths were used to calculate a NDVI according to Eq. 3, keeping only reflectance values of optimum quality (according to the MOD09Q1 Quality Control flag). Following Choler & al. (2010), we first removed outliers defined as NDVI values that were two times larger or smaller than the average value of the two preceding and the two following observations. Such sudden changes in NDVI are inconsistent with the growth or senescence dynamics of mountain grasslands and may be due to quality control issues, ephemeral snowfall during summer etc. Only 0.2% of the total NDVI values were discarded at this step. Missing values and removed outliers were gap-filled using a cubic spline interpolation. We then applied a Savitzky and Golay low pass filter in which the original data value at time t_i was replaced by the value of a cubic polynomial fitted for 2n+1 points, with n being the number of time steps preceding or following t_i (Savitzky and Golay, 1964). Consistent with our previous studies (Choler et al., 2010; 2015), we empirically found that a window size of seven days (i.e. n=3) was able to track ecologically significant changes in NDVI while still able to reduce noise in the NDVI time series efficiently. Finally, we used cubic splines to daily interpolate the NDVI time series and to derive the following phenological metrics (Fig. 2): (i) the growth onset, hereafter Onset, defined as the Julian day on which NDVI reached half its maximum, (ii) the NDVI maximum, hereafter NDVImax, as a proxy for the maximum canopy greenness, (iii) the Julian day of NDVImax, hereafter TNDVImax, as the date of the peak vegetation (iv) the absolute NDVI decrease during the 60 days following NDVImax, hereafter SEN (A60), see Eq. 4 as a proxy for the canopy senescence, and (v) the absolute NDVI increase during the 60 days following NDVImax, hereafter REG (A60), see Eq. 5 as a proxy for the end-of-season regrowth..

$$NDVI = \frac{\rho_{NIR} - \rho_{Red}}{\rho_{NIR} + \rho_{Red}} \quad (3)$$

$$SEN_A60 = \sum_{i=TNDVImax}^{TNDVImax+59} \text{abs}(\min(0, NDVI_{i+1} - NDVI_i)) \quad (4)$$

$$REG_A60 = \sum_{i=TNDVImax}^{TNDVImax+59} \max(0, NDVI_{i+1} - NDVI_i) \qquad (5)$$

182

183 Pixel-based estimates of phenology were averaged by elevation band and massif in order to
184 align with meteorological variables. For REG (A60) we transformed the raw values into binary data
185 (zero or positive values) and we calculated the percent of pixels exhibiting regrowth for each
186 combination of elevation band and massif.

187 Standard Major Axis (SMA) regression analysis was used to analyse the bivariate relationships
188 between anomalies of phenology and to test the statistical significance of any deviation of the slope
189 from unity and of the intercept from zero (Warton and Ormerod, 2007). We modelled anomalies of
190 NDVImax, SEN (A60) and REG (A60) as a linear function of anomalies of HWI and P-ET_0. The
191 model was written as follows (Eq. 6)

$$anom(Y_z) = \beta_{0,z} + \beta_{1,z}\, anom(P - ET_0)_z + \beta_{2,z} anom(HWI)_z + \varepsilon_z \qquad (6)$$

192

193 where *Y* is the dependent variable (phenology), β are the regression coefficients, *anom* means
194 standardized anomaly and ε is an error term. The β parameters were solved separately for each
195 elevation band (z) using ordinary least squares regression.

196 All statistical analyses were performed in *R* (R Core Team, 2017), using the *signal* library
197 (signal developers, 2013) for the time series analyses and the *raster* library (Hijmans, 2017) for the
198 spatial analysis. All figures were produced using the *ggplot2* (Wickham, 2016) and the *rasterVis*
199 (Perpinan Lamigueiro and Hijmans, 2018) libraries.

200

Results

Since the 1980s, warm to very warm summers with above normal HWI have become more frequent in the French Alps (Fig. 3A). The four summers with the highest HWI all occurred in the last 15 years, i.e. during the years 2003, 2012, 2015 and 2016 (Fig. 3A). The intensity of summer heat waves reached a maximum in 2003 with an HWI (JJA) median value of 184 for the 1950 m - 2250 m elevation band (Fig. S2A). During the same period, we found a wide range of water balance conditions during the summer period, with years when high values of HWI and negative P-ET_0 values co-occurred and other years when they occurred independently (Fig. 3, Fig. S2B). Summer droughts coincided with the 2003 and 2012 heat waves, while summer water balance was close to normal in 2015 and 2016 (Fig. 3B). The French Alps also experienced a severe drought in 2009, but this was not accompanied by a significant heat wave (Fig. 3B).

Figure 4 showed that the 2012 and 2016 heat waves mainly concerned the late season while those of 2003 and 2015 occurred throughout the growing season. Noticeably, there was no negative anomaly of P-ET_0 before the peak of biomass in 2015 (Fig. 4A) and only a moderate one after the peak (Fig. 4B). By comparison, the 2003, 2012 and 2016 late season heat waves co-occurred with dry conditions, with the most adverse situations taking place in 2003 and 2012 (Fig. 4B).

Plant growth onset in mountain grasslands typically occurred from the second half of April in the 1350 m 1650 m elevation band (mean DOY of 112) to the first half of June in the 2250 m 2550 m elevation band (mean DOY of 157) (Table 1). The date of maximum canopy greenness followed around 1.5 months later, with the length of the growing period (TNDVImax-ONSET) decreasing with elevation (Table 1). Late season phenology demonstrated a much larger range of inter-annual variability – with a coefficient of variation ranging from 18% to 31% for senescence and regrowth – as compared to those of Onset, TNDVImax and NDVImax (Table 1, Fig. 5), and this was observed across all elevation bands (Table 1). Overall, year-to-year variations in phenology were much smaller than those of HWI and P-ET_0 (Table 1).

The last four years (2013-2016) were among the five greenest summers of the study period, while the four strongest negative anomalies of NDVImax occurred before 2006 (Fig. 5D). The summers of 2003 and 2012 were characterized by an above normal senescence and a lack of regrowth, although the NDVImax was close to normal (Fig. 5D, E, F). A lack of regrowth was also observed in 2016, although senescence was close to normal and NDVImax was particularly high (Fig. 5D, E, F). By comparison, the year 2015 exhibited a below normal senescence and above normal regrowth and NDVImax (Fig. 5D, E, F).

Figure 6 shows the bivariate relationships among phenological anomalies and illustrates the particularity of the four years marked by heat wave occurrence. We found a strong positive relationship between anomalies of Onset and of TNDVImax (Table 2, Fig. 6A). The SMA slope was significantly below one indicating that maximum canopy greenness was reached in a shorter time in case of a delayed onset (Table 2). In addition, the two years with early season drought (e.g., 2003 and 2012) exhibited an earlier peak of NDVI than the one predicted by the SMA (Fig. 6A). The relationship between TNDVImax and NDVImax showed that a delayed phenology tend to be associated with higher values of NDVImax (Table 2, Fig. 6B). Remarkably, the two years with a pronounced early season heat wave (e.g., 2003 and 2015) exhibited a higher anomaly of NDVImax than predicted (Fig. 6B). Finally, we found a significant negative relationship between SEN (A60) and REG (A60) (Table 2, Fig. 6C). The years 2003, 2012 and 2016 exhibited a late-season phenology that was marked by normal to rapid senescence and limited regrowth while the year 2015 clearly showed an opposite pattern (Fig. 6C).

Finally, we examined the effects of HWI and P-ET_0 on phenology using multiple regression models. For this quantitative analysis, we distinguished between the two periods, i.e. before and after the peak, and among different elevation bands. Irrespective of elevation, there was a significant effect of P-ET_0 (B30) anomalies on NDVImax while no effect was detected for HWI (B30) (Table 3, Fig. 7A, B). Wetter conditions in the early season significantly enhanced the growth of grassland

while heat waves did not. P-ET_0 after the peak was also a significant driver of SEN (A60) and REG (A60) and the magnitude of this effect markedly differed among elevation bands. Wet summers significantly slowed down senescence and enhanced regrowth at low elevation, with up to 47% of variance explained in SEN (A60) and 24% of variance explained in REG (A60) in the 1350 m 1650 m elevation band (Table 3, Fig. 7C, E). These effects vanished higher up and became non-significant (SEN) or marginally significant (REG) above 2250 m (Table 3). Regarding HWI, we only found a significant and negative effect on senescence above 2250 m (Table 3). Noticeably, the effect of late-season heat waves on senescence depended on elevation with an increased senescence at low elevation (although not significantly) and a delayed senescence at high elevation (Fig. 7D).

Overall, these results indicated that maximum canopy greenness, senescence and regrowth were much more responsive to summer water balance than to heat waves. This is consistent with our initial hypotheses concerning the combined effects of heat wave and climatic water deficit on plant phenology. An early heat wave that did not coincide with a severe drought - as in 2015 and 2016 - did not significantly impact NDVImax. A late heat wave coinciding with a severe drought - as in 2003, 2012 and 2016 - resulted in an increased senescence and a low regrowth. A late heat wave not accompanied by a pronounced drought – as in 2015 - induced a delayed senescence, especially at high elevation, and a substantial regrowth.

Discussion

Our study of mountain grassland phenology in the French Alps for the period from 2000 to 2016 has provided the framework to analyse more thoroughly how these ecosystems respond to heat waves. Using data from the past two decades, we could show that (i) warmer summers generally have a positive effect on mountain canopy greenness especially at high elevation, (ii) water deficit hinders the positive temperature effect of heat waves on canopy greenness, and (iii) faster senescence and weaker late-season regrowth are the main negative effects of heat waves that co-occur with water deficit. Our findings emphasize the need to consider both the growth and senescent phases to

277 capture the effect of climate extremes on phenology. We also highlighted the pivotal role of the
278 magnitude of summer water balance and its within-summer distribution for understanding whether
279 mountain grasslands can benefit or not from higher summer temperatures.
280 We found a general increase in canopy greenness (NDVImax) in the French Alps during the study
281 period (2000-2016) which is consistent with our previous remote sensing study that showed a
282 greening trend for high-elevation ecosystems in the Ecrins Massif (Carlson et al., 2017). This
283 greening has also been documented in other temperate mountains (Xu et al., 2011) as well as in the
284 arctic and sub-arctic (Jia et al., 2003; Forbes et al., 2010). The combination of earlier snow melt-out
285 date and higher summer temperatures has been put forward as the main driver of changes in primary
286 productivity (Jonas et al., 2008; Zhang et al., 2013a; Choler, 2015; Dedieu et al., 2016; Choler,
287 2018). Besides temperature, other factors such as the increased deposition of atmospheric nitrogen
288 possibly led to some eutrophication of upland ecosystems and further contributed to greening
289 (Bowman et al., 2018). In alpine plants, nitrogen addition may induce stronger phenological changes
290 than warming alone (Smith et al., 2012). Our study indicated that sparsely vegetated meadows in the
291 French Alps are the most prone to greening, and we hypothesized that the prolonged growing season
292 in high-elevation contexts has created new thermally suitable niches for early plant colonizers which
293 could lead to an increase in primary productivity (Carlson et al., 2017). These conclusions are in
294 agreement with ground-based observations of community dynamics that emphasise the densification
295 of plant cover in open grasslands and/or the upward/northward shift of more productive functional
296 groups (Kullman, 2010; Myers-Smith et al., 2011; Steinbauer et al., 2018).
297 Our results also showed that the frequency of summer heat waves has increased over the last
298 decades in the French Alps. This is consistent with reports highlighting the increased probability of
299 heat waves in a warming climate (Stocker et al., 2013; Russo et al., 2014). We pointed out that the
300 four main heat waves that hit the Alps over the last 20 years did not have the same effect on
301 mountain grassland phenology. Remarkably, the 2015 heat wave had opposite late-season effects to

those of 2003, 2012, and 2016. This discrepancy is due to the combined effects of temperature and climatic water balance, both in magnitude and timing. Water deficit coincided with heat wave in 2003 and 2012, and to a lesser extent in 2016. We hypothesize that a threshold in the water balance was reached for these three years leading to the diminished canopy greenness during the late-season. Other reports have suggested that the disproportionate effect of the 2003 summer heat wave may not only be due to the unusually warm temperatures, but also to a negative soil water anomaly at the beginning of the growth period (Loew et al., 2009). Compared to the lowland ecosystems, mountain grasslands did not exhibit a strong reduction of NDVImax in 2003 and 2012, probably because the snowmelt provided sufficient water for the initial growth period, at least in the Northern Alps. Subsequently, the soil water content has likely decreased during the summer due to a climatic water deficit causing a significant reduction of canopy greenness during the late-season. For the year 2015, we hypothesize that the above normal water balance in the early season and the limited water deficit in the late-season have favoured the positive effect of the late-season heat wave, especially for the highest, i.e. the most temperature-limited, mountain grasslands. In their study of the 2003 heat wave, Jolly et al. (2005) reported marked regional differences in the response of high elevation ecosystems. In particular, it was striking that mountain ecosystems of the Southern Alps showed a reduced canopy greenness compared to the Northern French or Swiss Alps, which was likely related to the interplay of heat wave and water availability. Similarly, Cremonese et al. (2017) pointed out the co-limitation of high temperature and soil water content to impede the greening of a *Nardus*-rich grassland in 2015. Recent experimental studies conducted on temperate mountain grasslands showed that the direct effects of air temperature on photosynthesis and aboveground phytomass production strongly depend on soil water content (De Boeck et al., 2016). These findings should prompt us to improve our understanding and regional modelling of the soil water balance of mountain grasslands. Unfortunately, this remains notoriously difficult due to the many unknowns (e.g., the soil water capacity and lateral run-offs). However, with further temperature increases looming in the not so

distant future, there is an urgent need to formulate eco-hydrological models of seasonal leaf dynamics and to identify the different thresholds that drive ecosystem response. This is particularly true for grasslands of the subalpine belt that are the most sensitive to drought and are a key resource for summer livestock farming (Nettier et al., 2017)

Numerous studies on arctic and alpine ecosystems have underlined that the response to warming varies across functional groups (Arft et al., 1999; Jonas et al., 2008; Jung et al., 2014; Livensperger et al., 2016). In relation to the recent observed greening it is plausible that the expansion of more productive habitats has changed the responsiveness of mountain grasslands to climate extremes. The coexistence of a richer set of plant life forms may arise, e.g., through the migration of low shrubs onto the grasslands, or of tall perennial grasses into otherwise low-stature habitats. There are several lines of evidence that an increased functional diversity may provide some ecosystem insurance by buffering the impact of environmental changes (Diaz and Cabido, 2001). However, further studies are needed to examine a possible relationship between plant functional diversity and the phenological responses of mountain grasslands to heat waves and drought. For example, the combined use of high-resolution satellite imagery in combination with a regional-scale database of vegetation could provide new insights into this line of enquiry.

Our comparative analysis of mountain grassland phenology over the last two decades provides a knowledge base to help anticipate the long-term response of grasslands under future climate conditions. Regional climate models used to compute climate projections are operating at coarse resolutions (10-50 km) (Jacob et al., 2014) and are insufficient to provide ecologically-relevant surface parameters in mountainous regions (Ford et al., 2013). Although downscaling methods can refine projections of meteorological variables and snow cover dynamics (Verfaillie et al., 2018), further work is needed to translate these model outputs into bioclimatic indicators and assess to what extent they are driving canopy greenness. In the longer term, efforts have to be conducted towards prognostic models of mountain grassland phenology that capture both

352 temperature and soil water constraints. The dynamics of leaf growth and senescence remains poorly
353 represented in land surface models (Arora and Boer, 2005; Richardson et al., 2013), and this holds
354 particularly true for seasonally snow-covered mountain grasslands. Our study has focused on inter-
355 annual fluctuations to provide a broad picture over the French Alps. Further work examining
356 between-site phenological variation along elevational and bioclimatic gradients will provide a
357 complementary view and will be helpful to improve our representation of the feedback between
358 phenology and climate within process-oriented models.
359

Conclusions

Our study highlighted the combined effect of summer temperature and water balance on the phenology of temperate mountain grasslands. In the European Alps, the increased or prolonged canopy greenness of mountain grasslands that result from warmer conditions becomes less pronounced when water is limiting. While there has been a significant decadal-scale increase in both the summer temperature and the frequency of heat waves, summer precipitation and reference evapotranspiration did not show a similar trend and exhibited large inter-annual variability. In addition, there is a growing body of evidence to support long-term changes of mountain vegetation in relation to climate warming and land use change. The extent to which these changes modify the sensitivity of mountain grassland to extreme events will also be pivotal to make possible the prediction of canopy greenness under future climate.

Acknowledgements

Thanks are due to Brad Carlson for helpful discussions and to Deborah Verfaillie, Matthieu Lafaysse and Matthieu Vernay (CNRM/CEN) for maintenance and provision of the SAFRAN reanalysis used in this study. Comments and suggestions from the two reviewers have greatly improved the manuscript. This research was conducted within the Long-Term Socio-Ecological Research (LTSER) Zone Atelier Alpes, a member of the eLTER-Europe network. It received funding from the LTSER Zone Atelier Alpes and from a scholarship of CONACYT. LECA and CNRM/CEN are part of Labex OSUG@2020 (ANR10 LABX56).

381 **Tables**

382

383 **Table 1**. Annual means and inter-annual coefficients of variation (CV in %) of the meteorological

384 and phenological variables used in the study.

			Mean (CV)			
Metric	Period	Abbreviation	1350 m - 1650 m	1650 m - 1950 m	1950 m - 2250 m	2250 m - 2550 m
Meteorology						
	Summer	HWI (JJA)	55 (79)	65 (71)	58 (79)	45 (89)
Heat Wave magnitude Index	Preceding the peak	HWI (B30)	18 (76)	21 (77)	20 (107)	14 (127)
	Following the peak	HWI (A60)	35 (111)	43 (98)	34 (116)	22 (130)
Precipitation –	Summer	P-ET_0 (JJA)	61 (79)	58 (110)	51 (24)	16 (22)
Reference Crop	Preceding the peak	P-ET_0 (B30)	35 (150)	24 (135)	14 (98)	5 (-285)
Evapotranspiration (mm)	Following the peak	P-ET_0 (A60)	32 (25)	36 (-41)	39 (11)	25 (103)
Phenology						
Onset of growth (DOY)		ONSET	112 (8)	130 (8)	145 (8)	157 (7)
Date of maximum NDVI (DOY)		TNDVImax	175 (7)	184 (5)	192 (5)	200 (6)
Offset of growth (DOY)		OFFSET	327 (5)	315 (5)	306 (4)	300 (3)
Maximum NDVI		NDVImax	0.79 (2)	0.78 (2)	0.75 (3)	0.69 (4)
Senescence	Following the peak	SEN (A60)	0.13 (22)	0.14 (18)	0.16 (18)	0.19 (21)
Regrowth	Following the peak	REG (A60)	69 (18)	62 (19)	54 (24)	48 (31)

385

386 **Table 2**. Summary statistics for Standardized Major Axis (SMA) regression analysis of phenological
387 variables. Shown are correlation coefficients (r), estimates of slopes (a) and intercepts (b) with 95%
388 confidence intervals, Mean Square Error (MSE) and Mean Absolute Error (MAE). For the intercept,
389 (NS) indicates a non-significant offset. For the slope, (NS) indicates an estimate statistically
390 indistinguishable from one.

Relation	n	r	SMA intercept (b)	H_0: b=0 *P* value	SMA slope (a)	H_0: a=1 *P* value	MSE	MAE
ONSET - TNDVImax	1479	0.69	-0.11 (-0.13, -0.08)	***	0.73 (0.7, 0.76)	***	0.39	0.50
TNDVImax - NDVImax	1479	0.31	0.04 (0.01, 0.08)	*	0.97 (0.93, 1.02)	NS	0.51	0.55
SEN (A60) - REG (A60)	1478	-0.45	-0.1 (-0.16, -0.05)	***	-1.82 (-1.74, -1.91)	***	1.70	1.06

391

Table 3. Regression coefficients and adjusted R^2 for the linear models testing the effect of P-ET_0 and HWI on NDVImax, SEN (A60) and REG (A60). (x) denotes the interaction between the two effects. Plain text is for highly significant effect ($P < 0.001$), italics is for significant effect ($P < 0.01$). Empty cells indicate non-significant effects.

	NDVImax			
Effect	1350 m - 1650 m	1650 m - 1950 m	1950 m - 2250 m	2250 m - 2550 m
Intercept	-0.002	0.002	-0.043	-0.051
P-ET_0 (B30)	0.27	0.33	0.25	0.14
HWI (B30)				
P-ET_0 (B30) x HWI (B30)	0.16	0.15		
Adjusted R^2	0.14	0.16	0.11	0.04

	SEN (A60)				REG (A60)			
Effect	1350 m - 1650 m	1650 m - 1950 m	1950 m - 2250 m	2250 m - 2550 m	1350 m - 1650 m	1650 m - 1950 m	1950 m - 2250 m	2250 m - 2550 m
Intercept	-0.191	-0.147	-0.088	-0.042	0.108	0.016	-0.067	0.082
P-ET_0 (A60)	-0.37	-0.27	-0.20		0.57	0.59	0.51	*0.26*
HWI (A60)				-0.18				
P-ET_0 (A60) x HWI (A60)	-0.14	-0.08				*-0.06*	-0.21	
Adjusted R^2	0.47	0.33	0.08	0.05	0.24	0.24	0.20	0.05

Supplementary Table 1. Number of MODIS pixels by massif and elevation band.

	Elevation band				
Massif	1350 m - 1650 m	1650 m - 1950 m	1950 m - 2250 m	2250 m - 2550 m	Total
1. Chablais	553	787	119	*0*	**1459**
2. Aravis	878	679	94	*0*	**1651**
3. Mont-Blanc	174	728	714	49	**1665**
4. Bauges	268	233	*8*	*0*	**509**
5. Beaufortin	373	1425	1562	234	**3594**
6. Haute-Tarentaise	68	277	580	404	**1329**
7. Chartreuse	71	132	*1*	*0*	**204**
8. Belledonne	97	788	365	*4*	**1254**
9. Maurienne	296	1054	1179	430	**2959**
10. Vanoise	162	457	1572	899	**3090**
11. Haute-Maurienne	64	215	979	1181	**2439**
12. Grandes Rousses	415	1258	1529	622	**3824**
13. Thabor	75	274	717	636	**1702**
14. Vercors	561	324	*4*	*0*	**889**
15. Oisans	499	967	818	55	**2339**
16. Pelvoux	194	251	564	583	**1592**
17. Queyras	63	254	679	1489	**2485**
18. Devoluy	644	460	28	*1*	**1133**
19. Champsaur	601	651	918	419	**2589**
20. Embrunnais Parpaillon	113	165	523	454	**1255**
21. Ubaye	50	185	416	355	**1006**
22. Haut-Var Haut-Verdon	356	707	794	185	**2042**
23. Mercantour	342	946	1481	517	**3286**
Total	**6917**	**13217**	**15644**	**8517**	**44295**

Figure legends

Figure 1. (A) Study area showing the 23 SAFRAN massifs in the French Alps and the distribution of the 250 m-resolution MODIS pixels (n = 44,295) dominated by mountain grasslands. (B) Pixel distribution by massif and elevation band. Names of massifs are: 1. Chablais; 2. Aravis; 3. Mont-Blanc; 4. Bauges; 5. Beaufortin; 6. Haute-Tarentaise; 7. Chartreuse; 8. Belledonne; 9. Maurienne; 10. Vanoise; 11. Haute-Maurienne; 12. Grandes Rousses; 13. Thabor; 14. Vercors; 15. Oisans; 16. Pelvoux; 17. Queyras; 18. Devoluy; 19. Champsaur; 20. Embrunnais Parpaillon; 21. Ubaye; 22. Haut-Var Haut-Verdon; 23. Mercantour. Account of pixels by massif and elevation band is given in Fig. S2.

Figure 2. An idealized yearly course of vegetation index showing the different variables and periods that were used to capture the phenology of the mountain grasslands.

Figure 3. Annual standardized anomalies of (A) the Heat Wave magnitude Index (HWI (JJA)) and (B) the difference between precipitation and reference crop evapotranspiration (P-ET_0 (JJA)) during summer in mountain grasslands located between 1950 m and 2250 m. Meteorological variables were estimated using the SAFRAN reanalysis (see Materials and Methods for details). The study period of mountain grassland phenology started in year 2000 (dashed line). Boxplots represent the median (central bar), and the first and third quartiles, with whiskers showing the 95% confidence intervals. Grey boxplots represent the four main summer heat waves (2003, 2012, 2015, and 2016).

Figure 4. Bivariate plots of standardized anomalies of HWI and P-ET_0 during (A) the 30 days before (B30), and (B) the 60 days after (A60) the date of maximum NDVI (TNDVImax). Large dots represent the four main summer heat waves (2003, 2012, 2015, and 2016).

Figure 5. Annual standardized anomalies of mountain grassland phenology: (A) onset of growth, (B) date of maximum NDVI (TNDVImax), (C) offset of growth, (D) maximum canopy greenness (NDVImax), (E) senescence during the 60 days following NDVImax (SEN (A60)), and (F) regrowth during the 60 days following NDVImax (REG (A60)). Boxplots represent the median (central bar), and the first and third quartiles, with whiskers showing the 95% confidence intervals. Grey boxplots represent the four main summer heat waves (2003, 2012, 2015, and 2016).

Figure 6. Bivariate relationships between annual standardized anomalies of TNDVImax, NDVImax, SEN (A60) and REG (A60). Standard Major Axis (SMA) regression lines are shown. Large dots represent the four main summer heat waves (2003, 2012, 2015, and 2016).

Figure 7. Effect of HWI and P-ET_0 on: NDVImax (A, B), SEN (A60) (C, D) and REG (A60) (E, F). Dependent and independent variables used in the linear models are standardized anomalies. Anomalies of HWI have been log-transformed. Regression lines are shown for each elevation band (see Materials and Methods for details).

Supplementary Figure 1. Sensitivity of Heat Wave magnitude Index (HWI) to the length of the window (parameter n) used to estimate the threshold temperature value (Eq. 1 in Materials and Methods). Shown are the relative changes in HWI estimates when n varies from 15 days to 13 days (A), or from 15 days to 11 days (B).

Supplementary Figure 2. Annual time series of summer HWI and P-ET_0 for mountain grasslands located between 1950m and 2250m. Boxplots represent the median (central bar), and the first and

third quartiles, with whiskers showing the 95% confidence intervals. Grey boxplots represent the four main summer heat waves (2003, 2012, 2015, and 2016).

References

Allen, R.G., Pereira, L.S., Raes, D. and Smith, M., 1998. Crop evapotranspiration-Guidelines for computing crop water requirements-FAO Irrigation and drainage paper 56. FAO, Rome, 300: 6541.

Arft, A.M., Walker, M.D., Gurevitch, J., Alatalo, J.M., Bret Harte, M.S., Dale, M., Diemer, M., Gugerli, F., Henry, G.H.R., Jones, M.H., Hollister, R.D., Jonsdottir, I.S., Laine, K., Levesque, E., Marion, G.M., Molau, U., Molgaard, P., Nordenhall, U., Raszhivin, V., Robinson, C.H., Starr, G., Stenstrom, A., Stenstrom, M., Totland, O., Turner, P.L., Walker, L.J., Webber, P.J., Welker, J.M. and Wookey, P.A., 1999. Responses of tundra plants to experimental warming: Meta-analysis of the international tundra experiment. Ecol. Monogr., 69(4): 491-511.

Arora, V.K. and Boer, G.J., 2005. A parameterization of leaf phenology for the terrestrial ecosystem component of climate models. Global Change Biol., 11(1): 39-59.

Beniston, M., Farinotti, D., Stoffel, M., Andreassen, L.M., Coppola, E., Eckert, N., Fantini, A., Giacona, F., Hauck, C., Huss, M., Huwald, H., Lehning, M., Lopez-Moreno, J.-I., Magnusson, J., Marty, C., Moran-Tejeda, E., Morin, S., Naaim, M., Provenzale, A., Rabatel, A., Six, D., Stoetter, J., Strasser, U., Terzago, S. and Vincent, C., 2018. The European mountain cryosphere: a review of its current state, trends, and future challenges. Cryosphere, 12(2): 759-794.

Bowman, W.D., Ayyad, A., Bueno de Mesquita, C.P., Fierer, N., Potter, T.S. and Sternagel, S., 2018. Limited ecosystem recovery from simulated chronic nitrogen deposition. Ecological applications : a publication of the Ecological Society of America.

Cannone, N. and Pignatti, S., 2014. Ecological responses of plant species and communities to climate warming: upward shift or range filling processes? Clim. Change, 123(2): 201-214.

Carlson, B.Z., Corona, M.C., Dentant, C., Bonet, R., Thuiller, W. and Choler, P., 2017. Observed long-term greening of alpine vegetation-a case study in the French Alps. Environmental Research Letters, 12(11).

Choler, P., 2015. Growth response of temperate mountain grasslands to inter-annual variations in snow cover duration. Biogeosciences, 12(12): 3885-3897.

Choler, P., 2018. Winter soil temperature dependence of alpine plant distribution: Implications for anticipating vegetation changes under a warming climate. Perspectives in Plant Ecology Evolution and Systematics, 30: 6-15.

Choler, P., Sea, W., Briggs, P., Raupach, M. and Leuning, R., 2010. A simple ecohydrological model captures essentials of seasonal leaf dynamics in semi-arid tropical grasslands. Biogeosciences, 7(3): 907-920.

Cremonese, E., Filippa, G., Galvagno, M., Siniscalco, C., Oddi, L., di Cella, U.M. and Migliavacca, M., 2017. Heat wave hinders green wave: The impact of climate extreme on the phenology of a mountain grassland. Agric. For. Meteorol., 247: 320-330.

De Boeck, H.J., Bassin, S., Verlinden, M., Zeiter, M. and Hiltbrunner, E., 2016. Simulated heat waves affected alpine grassland only in combination with drought. New Phytol., 209(2): 531-541.

Dedieu, J.-P., Carlson, B.Z., Bigot, S., Sirguey, P., Vionnet, V. and Choler, P., 2016. On the Importance of High-Resolution Time Series of Optical Imagery for Quantifying the Effects of Snow Cover Duration on Alpine Plant Habitat. Remote Sensing, 8(6): 481-481.

Diaz, S. and Cabido, M., 2001. Vive la difference: plant functional diversity matters to ecosystem processes. Trends in Ecology and Evolution, 16(11): 646-655.

Dunn, A.H. and de Beurs, K.M., 2011. Land surface phenology of North American mountain environments using moderate resolution imaging spectroradiometer data. Remote Sens. Environ., 115(5): 1220-1233.

Durand, Y., Giraud, G., Laternser, M., Etchevers, P., Mérindol, L. and Lesaffre, B., 2009a. Reanalysis of 47 Years of Climate in the French Alps (1958–2005): Climatology and Trends for Snow Cover. Journal of Applied Meteorology and Climatology, 48(12): 2487-2512.

Durand, Y., Laternser, M., Giraud, G., Etchevers, P., Lesaffre, B. and Merindol, L., 2009b. Reanalysis of 44 Yr of Climate in the French Alps (1958-2002): Methodology, Model Validation, Climatology, and Trends for Air Temperature and Precipitation. Journal of Applied Meteorology and Climatology, 48(3): 429-449.

Fontana, F., Rixen, C., Jonas, T., Aberegg, G. and Wunderle, S., 2008. Alpine grassland phenology as seen in AVHRR, VEGETATION, and MODIS NDVI time series - a comparison with in situ measurements. Sensors, 8(4): 2833-2853.

Forbes, B.C., Macias Fauria, M. and Zetterberg, P., 2010. Russian Arctic warming and 'greening' are closely tracked by tundra shrub willows. Global Change Biol., 16(5): 1542-1554.

Ford, K.R., Ettinger, A.K., Lundquist, J.D., Raleigh, M.S. and Lambers, J.H.R., 2013. Spatial Heterogeneity in Ecologically Important Climate Variables at Coarse and Fine Scales in a High-Snow Mountain Landscape. Plos One, 8(6).

Gallinat, A.S., Primack, R.B. and Wagner, D.L., 2015. Autumn, the neglected season in climate change research. Trends Ecol. Evol., 30(3): 169-176.

Garonna, I., de Jong, R., Stockli, R., Schmid, B., Schenkel, D., Schimel, D. and Schaepman, M.E., 2018. Shifting relative importance of climatic constraints on land surface phenology. Environmental Research Letters, 13(2).

Gobiet, A., Kotlarski, S., Beniston, M., Heinrich, G., Rajczak, J. and Stoffel, M., 2014. 21st century climate change in the European Alps-A review. Sci. Total Environ., 493: 1138-1151.

Gottfried, M., Pauli, H., Futschik, A., Akhalkatsi, M., Barancok, P., Alonso, J.L.B., Coldea, G., Dick, J., Erschbamer, B., Calzado, M.R.F., Kazakis, G., Krajci, J., Larsson, P., Mallaun, M., Michelsen, O., Moiseev, D., Moiseev, P., Molau, U., Merzouki, A., Nagy, L., Nakhutsrishvili, G., Pedersen, B., Pelino, G., Puscas, M., Rossi, G., Stanisci, A., Theurillat, J.P., Tomaselli, M., Villar, L., Vittoz, P., Vogiatzakis, I. and Grabherr, G., 2012. Continent-wide response of mountain vegetation to climate change. Nature Climate Change, 2(2): 111-115.

Hijmans, R.J., 2017. raster: Geographic Data Analysis and Modeling. R package version 2.6-7. https://CRAN.R-project.org/package=raster.

Inglada, J., Vincent, A., Arias, M., Tardy, B., Morin, D. and Rodes, I., 2017. Operational High Resolution Land Cover Map Production at the Country Scale Using Satellite Image Time Series. Remote Sensing, 9(1).

Jacob, D., Petersen, J., Eggert, B., Alias, A., Christensen, O.B., Bouwer, L.M., Braun, A., Colette, A., Deque, M., Georgievski, G., Georgopoulou, E., Gobiet, A., Menut, L., Nikulin, G., Haensler, A., Hempelmann, N., Jones, C., Keuler, K., Kovats, S., Kroener, N., Kotlarski, S., Kriegsmann, A., Martin, E., van Meijgaard, E., Moseley, C., Pfeifer, S., Preuschmann, S., Radermacher, C., Radtke, K., Rechid, D., Rounsevell, M., Samuelsson, P., Somot, S., Soussana, J.-F., Teichmann, C., Valentini, R., Vautard, R., Weber, B. and Yiou, P., 2014. EURO-CORDEX: new high-resolution climate change projections for European impact research. Regional Environmental Change, 14(2): 563-578.

Jia, G.S.J., Epstein, H.E. and Walker, D.A., 2003. Greening of arctic Alaska, 1981-2001. Geophys. Res. Lett., 30(20).

Jolly, W.M., Dobbertin, M., Zimmermann, N.E. and Reichstein, M., 2005. Divergent vegetation growth responses to the 2003 heat wave in the Swiss Alps. Geophys. Res. Lett., 32(18): NIL_1-NIL_4.

Jonas, T., Rixen, C., Sturm, M. and Stoeckli, V., 2008. How alpine plant growth is linked to snow cover and climate variability. Journal of Geophysical Research-Biogeosciences, 113(G3).

Jung, V., Albert, C.H., Violle, C., Kunstler, G., Loucougaray, G. and Spiegelberger, T., 2014. Intraspecific trait variability mediates the response of subalpine grassland communities to extreme drought events. J. Ecol., 102(1): 45-53.

Kullman, L., 2010. Alpine flora dynamics - a critical review of responses to climate change in the Swedish Scandes since the early 1950s. Nord. J. Bot., 28(4): 398-408.

Lenoir, J., Gegout, J.C., Marquet, P.A., de Ruffray, P. and Brisse, H., 2008. A significant upward shift in plant species optimum elevation during the 20th century. Science, 320(5884): 1768-1771.

Liu, Q., Piao, S.L., Janssens, I.A., Fu, Y.S., Peng, S.S., Lian, X., Ciais, P., Myneni, R.B., Penuelas, J. and Wang, T., 2018. Extension of the growing season increases vegetation exposure to frost. Nature Communications, 9.

Livensperger, C., Steltzer, H., Darrouzet-Nardi, A., Sullivan, P.F., Wallenstein, M. and Weintraub, M.N., 2016. Earlier snowmelt and warming lead to earlier but not necessarily more plant growth. Aob Plants, 8.

Loew, A., Holmes, T. and de Jeu, R., 2009. The European heat wave 2003: Early indicators from multisensoral microwave remote sensing? Journal of Geophysical Research-Atmospheres, 114.

Marchin, R.M., McHugh, I., Simpson, R.R., Ingram, L.J., Balas, D.S., Evans, B.J. and Adams, M.A., 2018. Productivity of an Australian mountain grassland is limited by temperature and dryness despite long growing seasons. Agric. For. Meteorol., 256: 116-124.

Myers-Smith, I.H., Forbes, B.C., Wilmking, M., Hallinger, M., Lantz, T., Blok, D., Tape, K.D., Macias-Fauria, M., Sass-Klaassen, U., Levesque, E., Boudreau, S., Ropars, P., Hermanutz, L., Trant, A., Collier, L.S., Weijers, S., Rozema, J., Rayback, S.A., Schmidt, N.M., Schaepman-Strub, G., Wipf, S., Rixen, C., Menard, C.B., Venn, S., Goetz, S., Andreu-Hayles, L., Elmendorf, S., Ravolainen, V., Welker, J., Grogan, P., Epstein, H.E. and Hik, D.S., 2011. Shrub expansion in tundra ecosystems: dynamics, impacts and research priorities. Environmental Research Letters, 6(4).

Nettier, B., Dobremez, L., Lavorel, S. and Brunschwig, G., 2017. Resilience as a framework for analyzing the adaptation of mountain summer pasture systems to climate change. Ecol. Soc., 22(4).

Perpinan Lamigueiro, O. and Hijmans, R., 2018. rasterVis. R package version 0.45. URL: http://oscarperpinan.github.io/rastervis/.

Pettorelli, N., Vik, J.O., Mysterud, A., Gaillard, J.M., Tucker, C.J. and Stenseth, N.C., 2005. Using the satellite-derived NDVI to assess ecological responses to environmental change. Trends Ecol. Evol., 20(9): 503-510.

R Core Team, 2017. R: A language and environment for statistical computing. http://www.R-project.org/. R Foundation for Statistical Computing, Vienna, Austria.

Richardson, A.D., Keenan, T.F., Migliavacca, M., Ryu, Y., Sonnentag, O. and Toomey, M., 2013. Climate change, phenology, and phenological control of vegetation feedbacks to the climate system. Agric. For. Meteorol., 169: 156-173.

Russo, S., Dosio, A., Graversen, R.G., Sillmann, J., Carrao, H., Dunbar, M.B., Singleton, A., Montagna, P., Barbola, P. and Vogt, J.V., 2014. Magnitude of extreme heat waves in present climate and their projection in a warming world. Journal of Geophysical Research-Atmospheres, 119(22): 12500-12512.

Savitzky, A. and Golay, M.J.E., 1964. Smoothing and Differentiation of Data by Simplified Least Squares Procedures. Analytical Chemistry, 36: 1627-1639.

signal developers, 2013. signal: Signal processing. URL: http://r-forge.r-project.org/projects/signal/.

Smith, J.G., Sconiers, W., Spasojevic, M.J., Ashton, I.W. and Suding, K.N., 2012. Phenological Changes in Alpine Plants in Response to Increased Snowpack, Temperature, and Nitrogen. Arctic Antarctic and Alpine Research, 44(1): 135-142.

Steinbauer, M.J., Grytnes, J.-A., Jurasinski, G., Kulonen, A., Lenoir, J., Pauli, H., Rixen, C., Winkler, M., Bardy-Durchhalter, M., Barni, E., Bjorkman, A.D., Breiner, F.T., Burg, S., Czortek, P., Dawes, M.A., Delimat, A., Dullinger, S., Erschbamer, B., Felde, V.A., Fernandez-Arberas, O., Fossheim, K.F., Gomez-Garcia, D., Georges, D., Grindrud, E.T., Haider, S., Haugum, S.V., Henriksen, H., Herreros, M.J., Jaroszewicz, B., Jaroszynska, F., Kanka, R., Kapfer, J., Klanderud, K., Kuhn, I., Lamprecht, A., Matteodo, M., di Cella, U.M., Normand, S., Odland, A., Olsen, S.L., Palacio, S., Petey, M., Piscova, V., Sedlakova, B., Steinbauer, K., Stockli, V., Svenning, J.-C., Teppa, G., Theurillat, J.-P., Vittoz, P., Woodin, S.J., Zimmermann, N.E. and Wipf, S., 2018. Accelerated increase in plant species richness on mountain summits is linked to warming. Nature, 556(7700): 231-+.

Stocker, T.F., Qin, D., Plattner, G., Tignor, M., Allen, S., Boschung, J., Nauels, A., Xia, Y., Bex, V. and Midgley, P., 2013. Climate change 2013: the physical science basis. Intergovernmental panel on climate change, working group I contribution to the IPCC fifth assessment report (AR5). New York.

Vannier, O. and Braud, I., 2012. Calcul d'une évapotranspiration de référence spatialisée pour la modélisation hydrologique à partir des données de la réeanalyse SAFRAN de Météo-France.

https://irsteadoc.irstea.fr/cemoa/PUB00029135. Rapport scientifique, Note de travail du plateau SOMME (Synergie Observation Modélisation en Modélisation de l'Environnement) d'Envirhônalp.

Verfaillie, D., Lafaysse, M., Deque, M., Eckert, N., Lejeune, Y. and Morin, S., 2018. Multi-component ensembles of future meteorological and natural snow conditions for 1500m altitude in the Chartreuse mountain range, Northern French Alps. Cryosphere, 12(4): 1249-1271.

Warton, D. and Ormerod, J., 2007. smatr: (Standardised) Major Axis Estimation and Testing Routines. R package version 2.1. http://web.maths.unsw.edu.au/~dwarton.

Wheeler, J.A., Hoch, G., Cortes, A.J., Sedlacek, J., Wipf, S. and Rixen, C., 2014. Increased spring freezing vulnerability for alpine shrubs under early snowmelt. Oecologia, 175(1): 219-229.

Wickham, H., 2016. ggplot2: Elegant Graphics for Data Analysis. Springer-Verlag New York, 2016.

Xu, W.X., Gu, S., Zhao, X.Q., Xiao, J.S., Tang, Y.H., Fang, J.Y., Zhang, J. and Jiang, S., 2011. High positive correlation between soil temperature and NDVI from 1982 to 2006 in alpine meadow of the Three-River Source Region on the Qinghai-Tibetan Plateau. International Journal of Applied Earth Observation and Geoinformation, 13(4): 528-535.

Zhang, G., Zhang, Y., Dong, J. and Xiao, X., 2013a. Green-up dates in the Tibetan Plateau have continuously advanced from 1982 to 2011. Proc. Natl. Acad. Sci. U.S.A., 110(11): 4309-4314.

Zhang, L., Guo, H., Ji, L., Lei, L., Wang, C., Yan, D., Li, B. and Li, J., 2013b. Vegetation greenness trend (2000 to 2009) and the climate controls in the Qinghai-Tibetan Plateau. Journal of Applied Remote Sensing, 7.

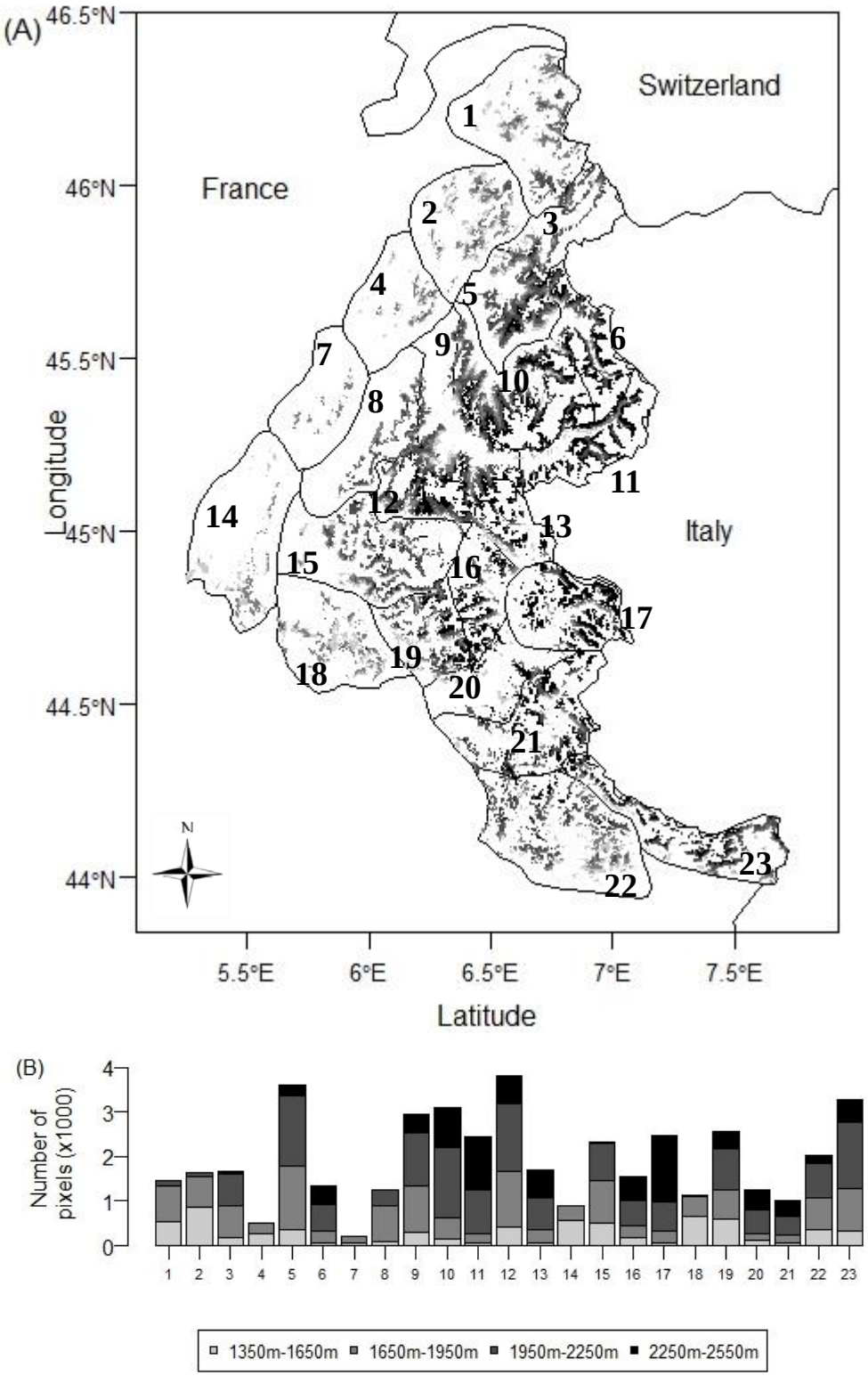

(A)
46.5°N
46°N
45.5°N
45°N
44.5°N
44°N
Longitude
5.5°E
6°E
6.5°E
7°E
7.5°E
Latitude
Switzerland
France
Italy
N
1
2
3
4
5
6
7
8
9
10
11
12
13
14
15
16
17
18
19
20
21
22
23
(B)
Number of pixels (x1000)
0
1
2
3
4
1350m-1650m
1650m-1950m
1950m-2250m
2250m-2550m

Figure 1

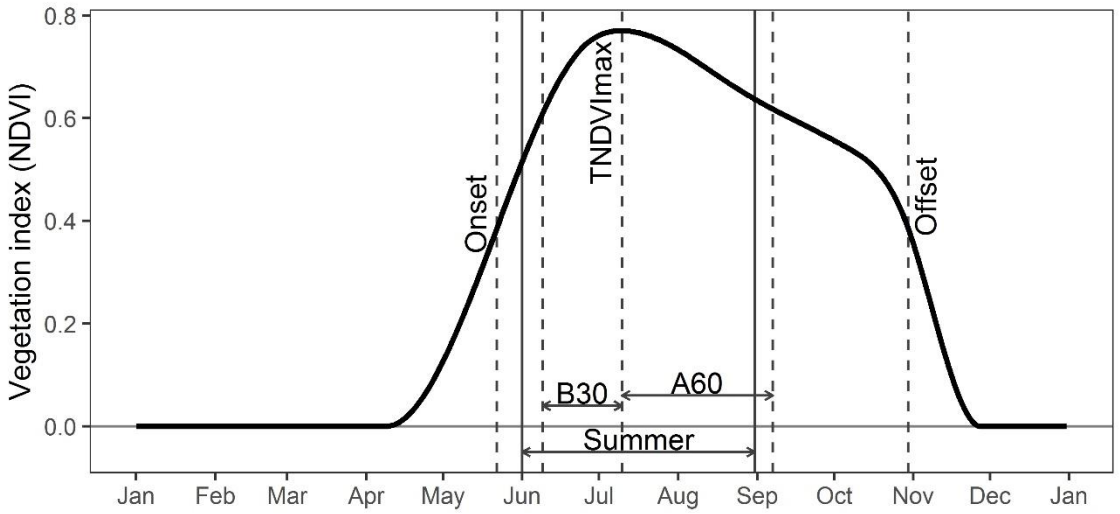

Vegetation index (NDVI)
0.8
0.6
0.4
0.2
0.0
Onset
TNDVImax
Offset
B30
A60
Summer
Jan
Feb
Mar
Apr
May
Jun
Jul
Aug
Sep
Oct
Nov
Dec
Jan

Figure 2

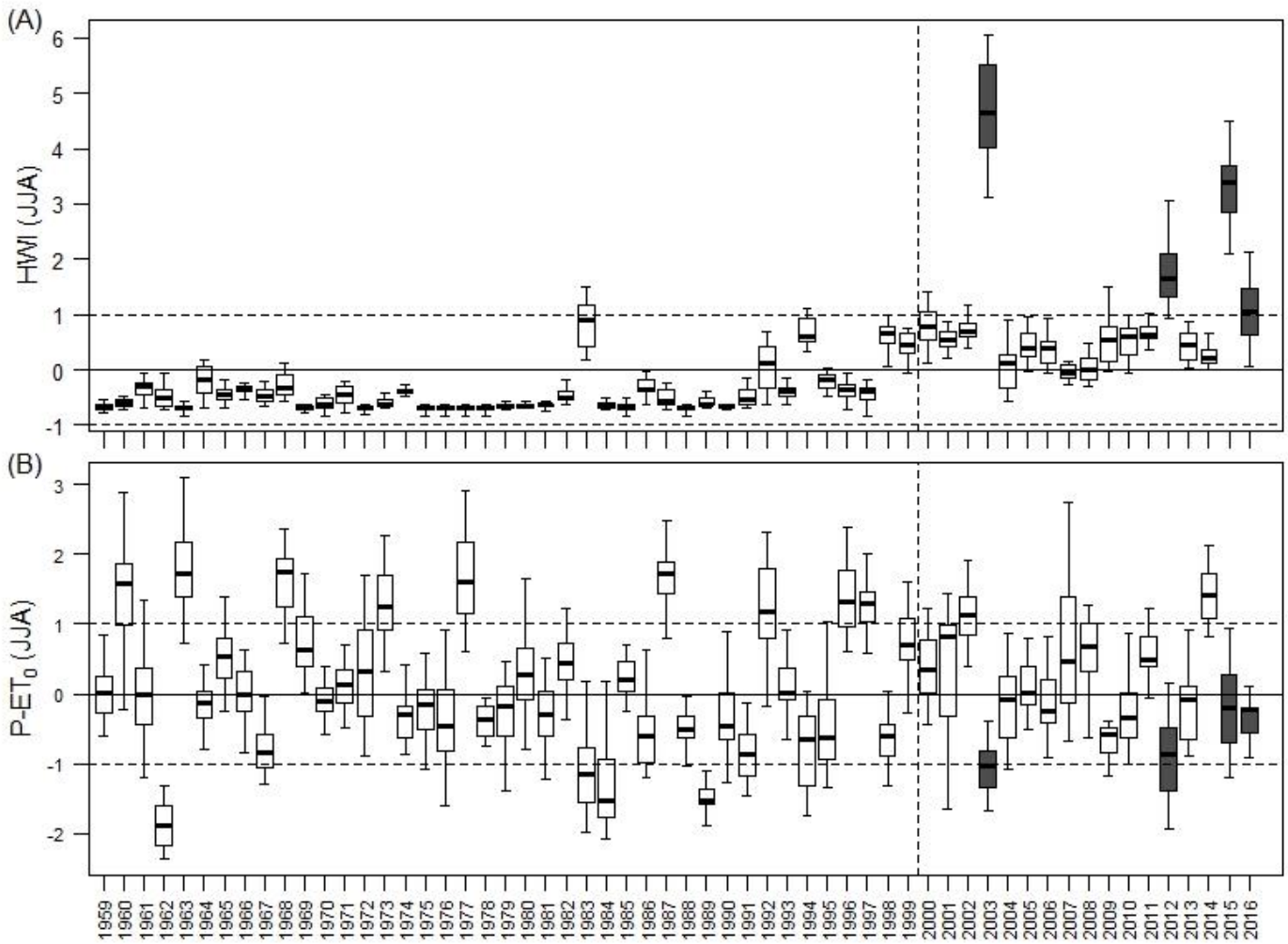

(A)
HWI (JJA)
6
5
4
3
2
1
0
-1
(B)
P-ET0 (JJA)
3
2
1
0
-1
-2
1959
1960
1961
1962
1963
1964
1965
1966
1967
1968
1969
1970
1971
1972
1973
1974
1975
1976
1977
1978
1979
1980
1981
1982
1983
1984
1985
1986
1987
1988
1989
1990
1991
1992
1993
1994
1995
1996
1997
1998
1999
2000
2001
2002
2003
2004
2005
2006
2007
2008
2009
2010
2011
2012
2013
2014
2015
2016

Figure 3

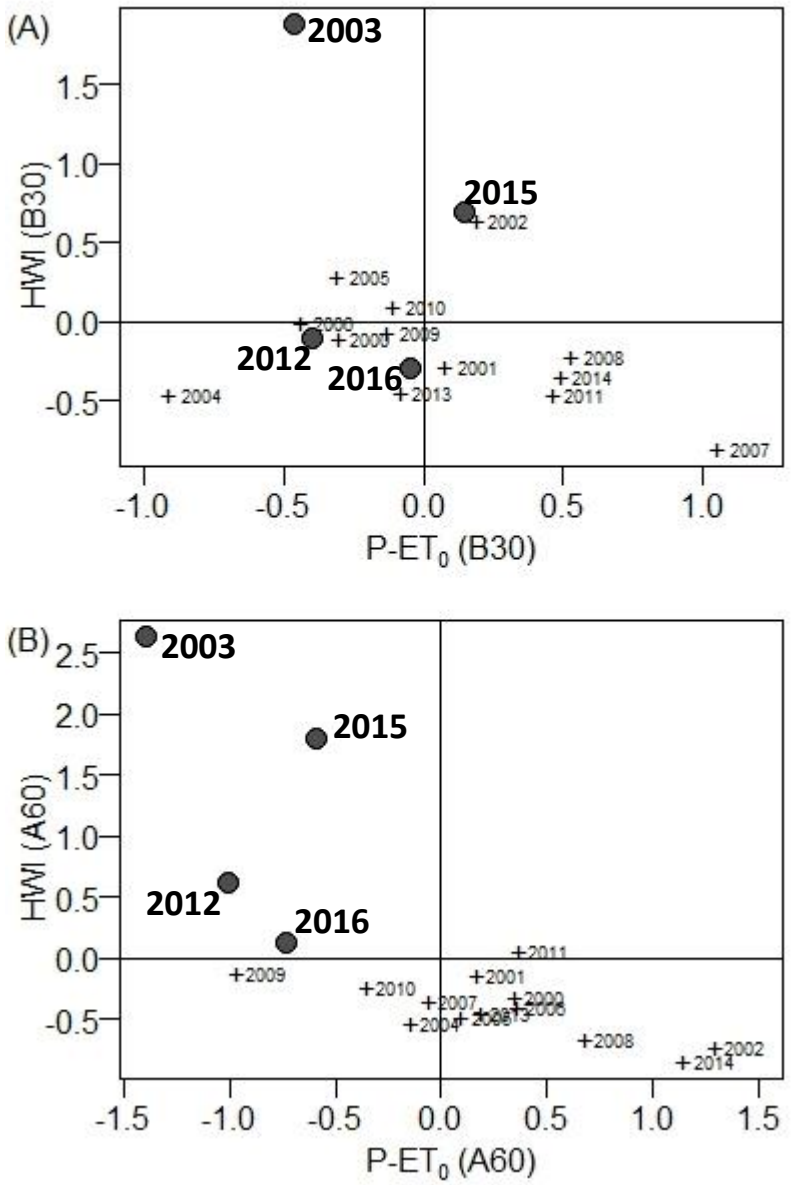

(A)
2003
2015
2012
2016
2002
2005
2010
2000
2009
2006
2001
2008
2014
2004
2013
2011
2007
HWI (B30)
P-ET0 (B30)
(B)
2003
2015
2012
2016
2011
2009
2001
2010
2007
2004
2008
2002
2014
HWI (A60)
P-ET0 (A60)

Figure 4

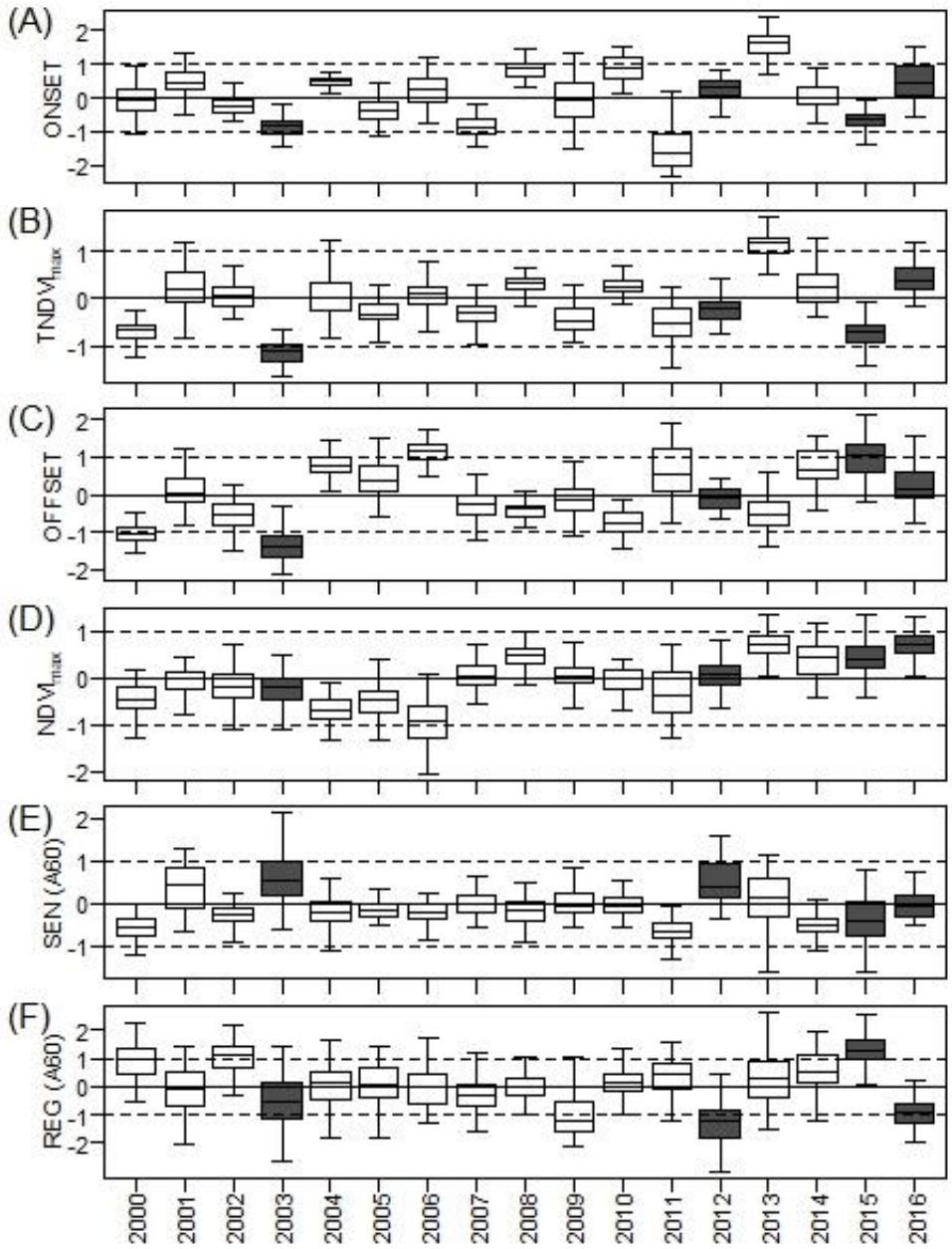

(A)
ONSET
(B)
TNDVI$_{max}$
(C)
OFFSET
(D)
NDVI$_{max}$
(E)
SEN (A60)
(F)
REG (A60)
2000
2001
2002
2003
2004
2005
2006
2007
2008
2009
2010
2011
2012
2013
2014
2015
2016

Figure 5

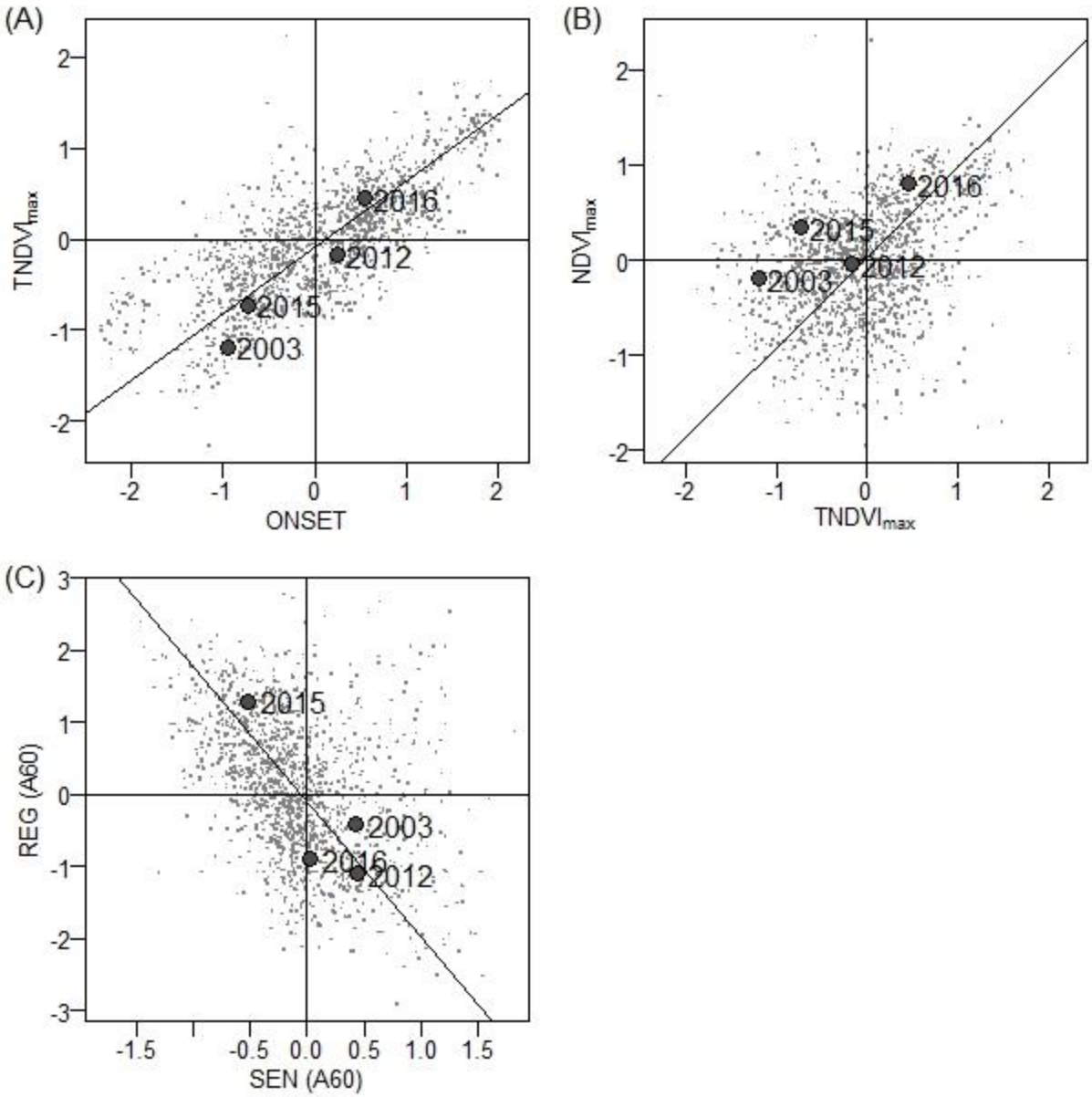

(A)
TNDVI$_{max}$
ONSET
2016
2012
2015
2003
(B)
NDVI$_{max}$
TNDVI$_{max}$
2016
2015
2012
2003
(C)
REG (A60)
SEN (A60)
2015
2003
2016
2012

Figure 6

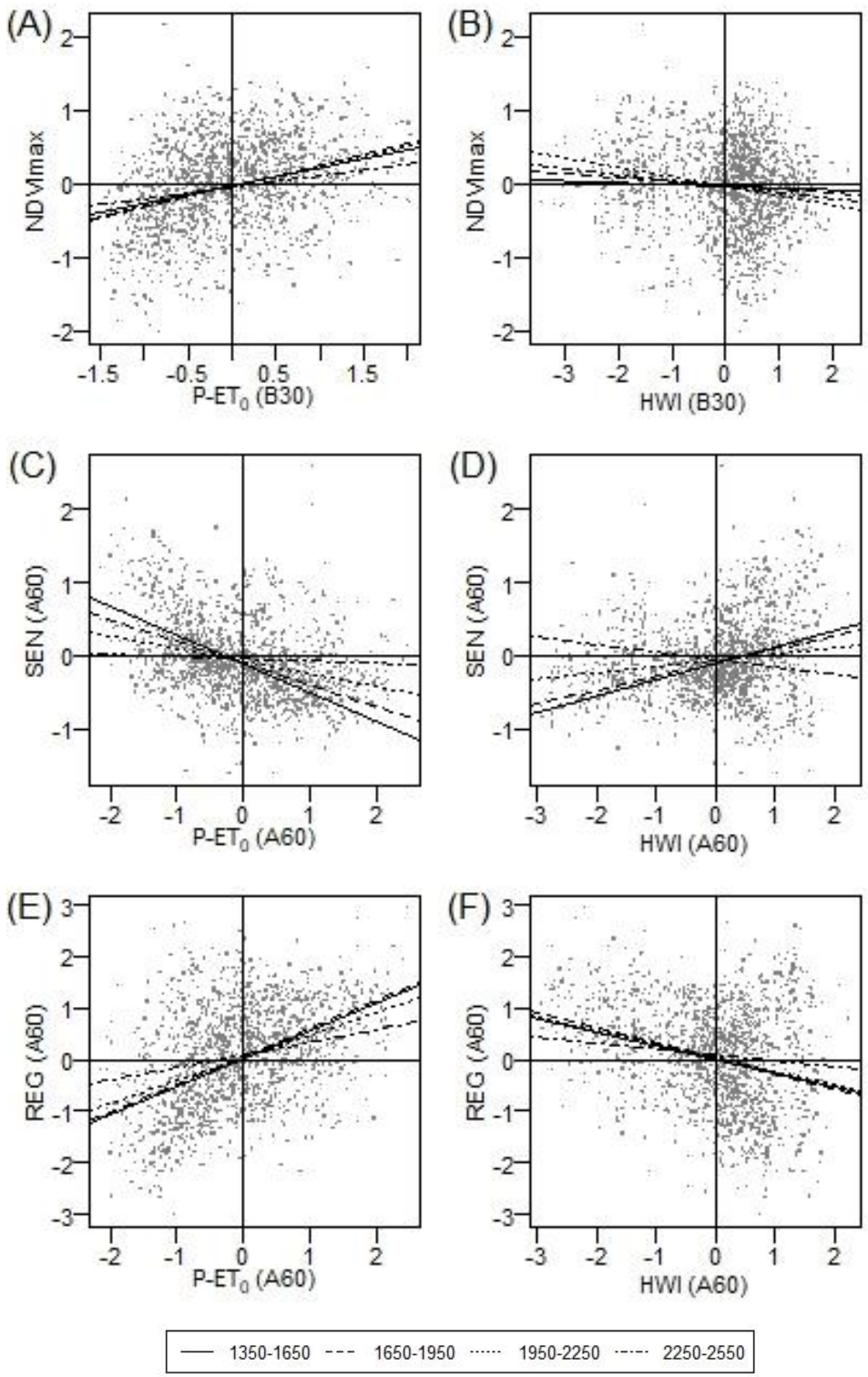
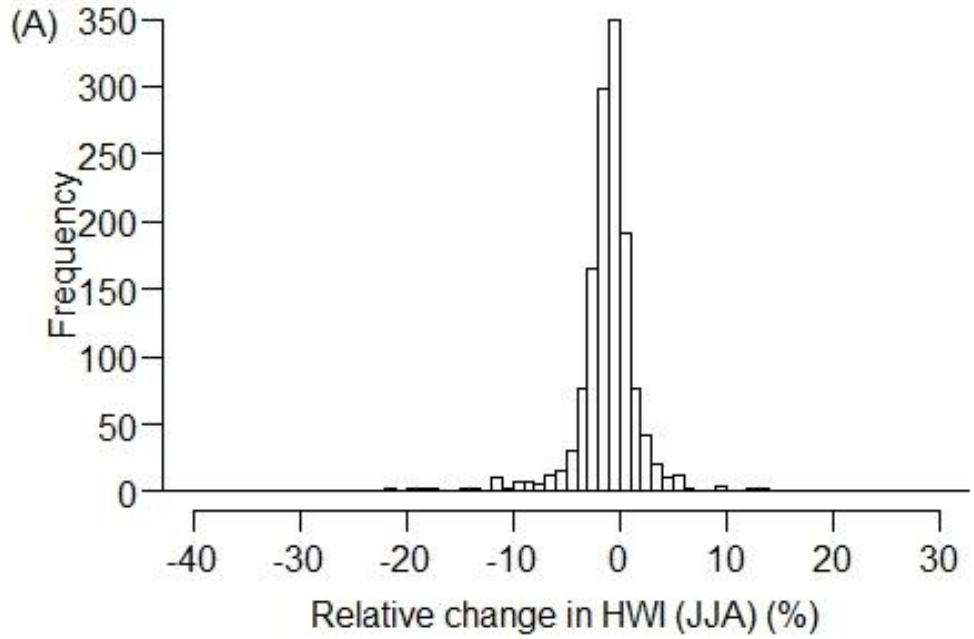

(A)
NDVImax
P-ET0 (B30)
(B)
NDVImax
HWI (B30)
(C)
SEN (A60)
P-ET0 (A60)
(D)
SEN (A60)
HWI (A60)
(E)
REG (A60)
P-ET0 (A60)
(F)
REG (A60)
HWI (A60)
1350-1650
1650-1950
1950-2250
2250-2550

Figure 7


(A)
350
300
250
200
150
100
50
0
Frequency
-40
-30
-20
-10
0
10
20
30
Relative change in HWI (JJA) (%)

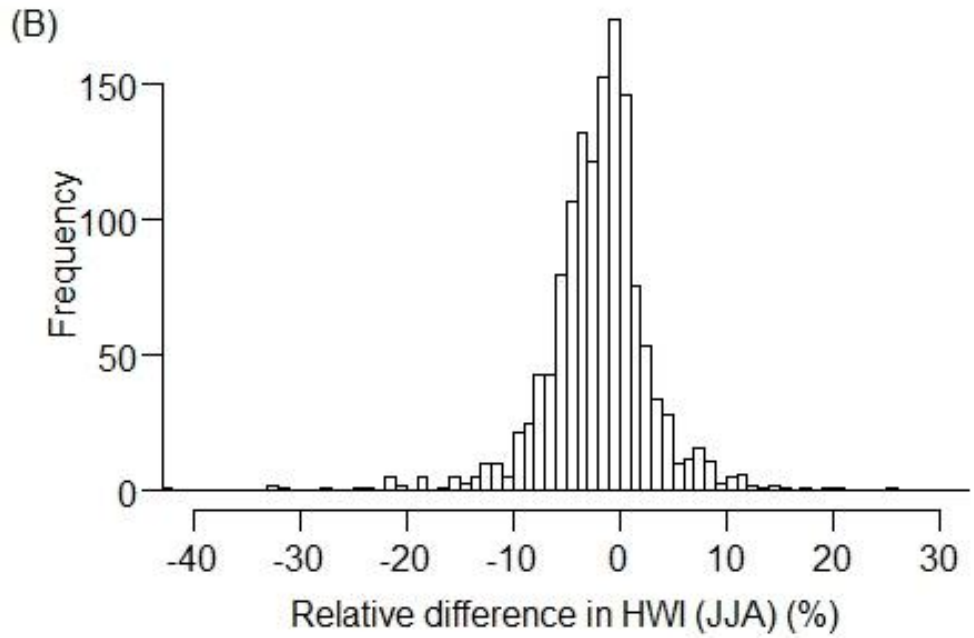

(B)
150
100
50
0
Frequency
-40
-30
-20
-10
0
10
20
30
Relative difference in HWI (JJA) (%)

Figure S1

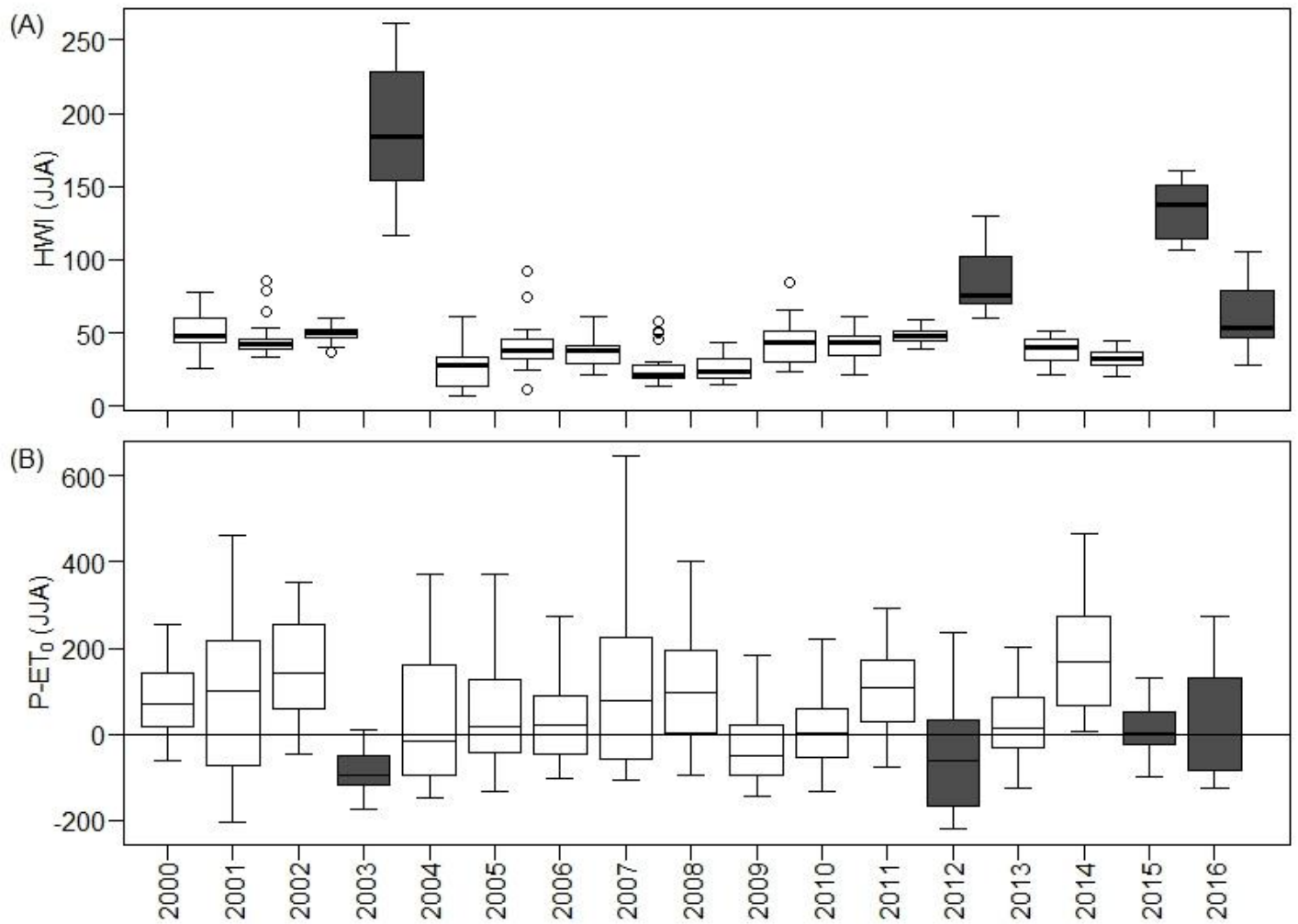

(A)
HWI (JJA)
250
200
150
100
50
0
(B)
P-ET0 (JJA)
600
400
200
0
-200
2000
2001
2002
2003
2004
2005
2006
2007
2008
2009
2010
2011
2012
2013
2014
2015
2016

Figure S2